Flow of Foams

Katgert, G.

Chapter 1

Introduction

An aqueous foam consists of gas bubbles dispersed in water which contains a stabilising agent (surfactant). Despite the simplicity of its composition, the properties of a foam are in general quite complex [1]. The static structure and the ageing of a foam is reasonably well understood, while the behaviour of foams under forcing, i.e. the elasticity and the rheology, has only recently received attention. This is at least partly due to the introduction of the jamming phase diagram [2], which has lead to an upsurge of experimental and theoretical work in the entire field of soft condensed matter physics. The rheology of foams, and of emulsions, which are very closely related to foams but consist of bubbles of an immiscible fluid phase instead of a gas, is expected to obey this jamming picture and the absence of solid friction in both systems would allow for a connection between experiment and simulations.

To investigate foam rheology and connect the bulk behaviour with the motion of the individual bubbles, we will investigate monolayers of foam bubbles which float on the surface of a surfactant solution and which allow for direct imaging of the constituent particles.

However, in order to be able to understand the rheology of foams it is necessary that we first understand the microscopic origin of the rheological properties of individual bubbles. Only then can we try to understand the collective behaviour of collections of these bubbles. The following treatment is focussed on foams, but is equally well valid for emulsions, except for a few details, which are discussed in section 1.4.2.

1.1 Microscopics: Foam films, stability

In this section we discuss the chemical components that make up a foam and their influence on the various processes that lead to stabilisation and structural evolution of a foam.

1.1.1 Surfactants and surface tension

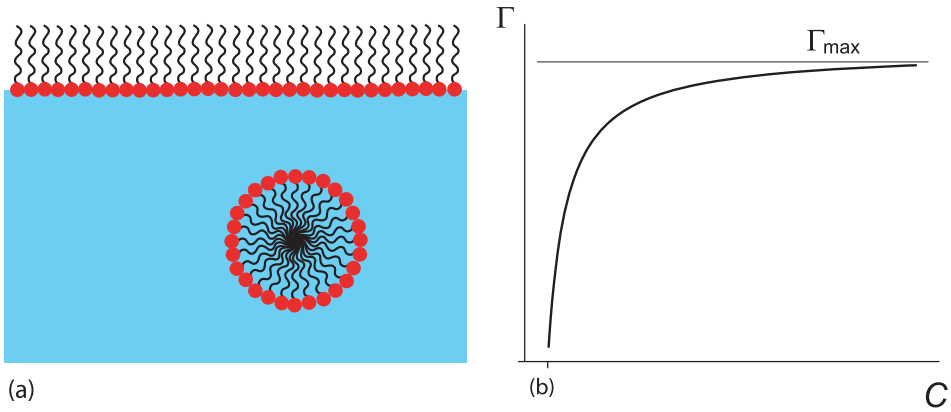

FIGURE 1.1: (a) Surfactant molecules adsorbed at the interface. At the CMC the surface is maximally covered by surfactant molecules and micelles start to form. (b) Langmuir adsorption isotherm, relating the surface concentration Γ to the bulk concentration C [3].

Foam bubbles are generally stabilised against rupture and coalescence by a special class of molecules called surfactants (**surf**ace **act**ive **a**ge**nts**). These molecules consist of a hydrophilic (polar) head group and a hydrophobic (apolar) tail. When these molecules are dissolved in the water phase they spontaneously adsorb at the interface. The head group sits in the water phase and the tail points towards the oil phase (in case of an emulsion) or the gas phase (in case of a foam). As a result the surfactant molecules lower the surface tension σ of an interface, which can be understood as follows: a surface energy arises because the water molecules at the interface are missing bonds. The liquid seeks to minimise the excess energy associated with these missing bonds and hence minimises its surface area, leading to a surface tension. The surfactants lower the excess

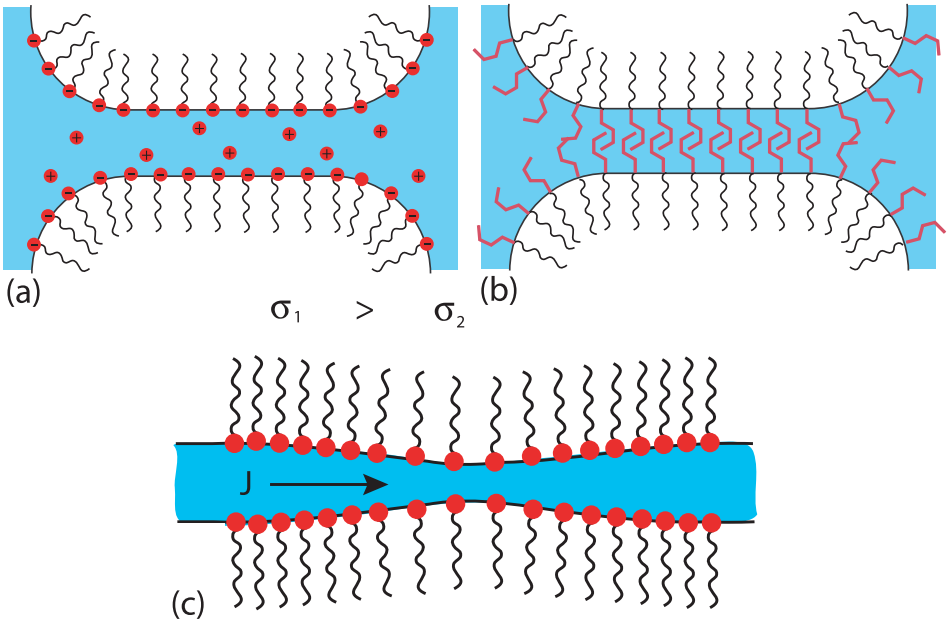

FIGURE 1.2: Static and dynamic foam stabilisation: (a) electrostatic and (b) steric repulsion of the surfactant monolayers provide static foam stabilisation while (c) dynamic stabilisation against fluctuations is guaranteed by the Marangoni effect, which is the coupling between surface tension gradients and flow in the liquid.

energy of missing bonds and hence lower the surface tension.

Besides being polar, the headgroup of a surfactant molecule can be charged or uncharged. Charged surfactants are called *ionic surfactants* and either have a negatively (anionic), a positively (cationic), or both negatively and positively (amphoteric) charged head group. A much used anionic surfactant is Sodium Dodecyl Sulfate (SDS). Uncharged surfactants are called *non-ionic surfactants*. An often used non-ionic surfactant of low molecular weight is polyoxyethylene sorbitan monolaurate, which is better known under its trade name Tween 20. Other important classes of non-ionic surfactants are the synthetic polymeric surfactants such as Pluronic and the natural polymeric surfactants (proteins) such as Bovine Serum Albumin and Casein.

The surface tension σ, the bulk concentration C and the surface con-

centration Γ are related through the Gibbs-Duhem equation for the surface phase [3]:

$$d\sigma = \Gamma k_B T d(\ln C). \tag{1.1}$$

In order to calculate $\sigma(C)$, a model adsorption isotherm is chosen, such as the Langmuir adsorption isotherm shown in Fig. 1.1(b) :

$$\Gamma(C) = \Gamma_{max} \frac{KC}{1+KC}, \tag{1.2}$$

where K is an adsorption constant. Eq. (1.1) can now be integrated to obtain the dependence of surface tension on bulk concentration.

When increasing the surfactant concentration in the liquid phase (the bulk concentration C), the surface concentration increases according to Eq. (1.1) until the bulk concentration reaches the critical micelle concentration (CMC). By further increasing the bulk concentration, the surfactant molecules form micelles which are spherical shapes or bilayers with the polar heads pointing towards the surrounding liquid and the apolar tails grouped together and shielded against interaction with the fluid by the heads, see Fig. 1.1, in order to minimise binding energy. At the CMC, the chemical potential for surfactants to adsorb at the surface or form micelles is equal and for concentrations above the CMC, the surface concentration can only be increased and hence the surface tension can only be reduced by decrasing the repulsive interaction between the surfactant molecules, for instance by adding electrolyte such that the molecules pack closer at the surface.

The Gibbs surface elasticity, which is in fact a two dimensional elastic modulus (units N/m) and is given by [3]

$$E_G = -\frac{d\sigma}{d(ln\Gamma)}, \tag{1.3}$$

describes the response of the surface tension to variations in the surface concentration. A surfactant layer with a high Gibbs elasticity experiences large changes in surface tension for small variations in surface concentration. Local fluctuations in the surface concentration are energetically strongly unfavourable and result in large stresses. For such a surfactant layer, these fluctuations will mainly be damped by the Marangoni effect, which is the flow of fluid from regions of low surface tension to regions of

high surface tension as a result of the coupling of the surface stress to the fluid below through viscosity.

In order to be able to understand how surfactants stabilise foams we now have to consider the thin soap film between two neighbouring foam bubbles. The thin film consists of two monolayers of surfactant molecules with the bulk phase in between. Both in ionic and in non-ionic surfactants, static stabilisation is achieved by repulsive forces between the surfactant monolayers. For ionic surfactants the repulsive force is electrostatic and is caused by the charged groups at the interfaces , whereas for nonionic surfactants, static stabilisation is achieved by a steric repulsion, which is due to the overlap of the polymer chains, see Fig. 1.2 (a,b).

Dynamic stabilisation against fluctuations in the film thickness is ensured by the Marangoni effect, see Fig. 1.2 (c). If the film locally thins it curves inwards, its area locally increases and the surface tension becomes higher at the dimple but the resulting bulk flow towards the dimple restores the equilibrium thickness. A dimple (thicker region) in the film will by the same mechanism grow further, but the diffusion of surfactant molecules to the dimple will eventually stop this.

1.1.2 Microscopic nature of foam evolution

When no mechanical forcing is applied, foams evolve due to *drainage*, *coarsening* and *coalescence*. Drainage is caused by gravity which leads to a downward flow of the liquid phase, coarsening is caused by gas diffusion between neighbouring bubbles, while rupture of the flat films may cause coalescence between bubbles. We will now discuss how these processes are affected by the constituents of the foam.

Drainage. An increase of viscosity of the liquid phase, for instance by adding glycerol, can help to decrease the drainage velocity, but the speed at which a foam drains is mainly affected by the composition of the surfactants at the interfaces. We have introduced the Gibbs elasticity above, and connected to this we can define a surface elastic modulus as well as a surface viscosity that describe the energy cost of the stretching and shearing of interfaces. These moduli depend on how easily surfactant molecules diffuse from the bulk to the interfaces and vice versa, and the interfaces are either said to be *mobile* (low E_G, ≈ 0 mN/m) or *immobile* (high E_G, ≈ 50 mN/m). A flow of bulk liquid along a soap film couples to the surfactant molecules and results in surface tension gradients. If the film is

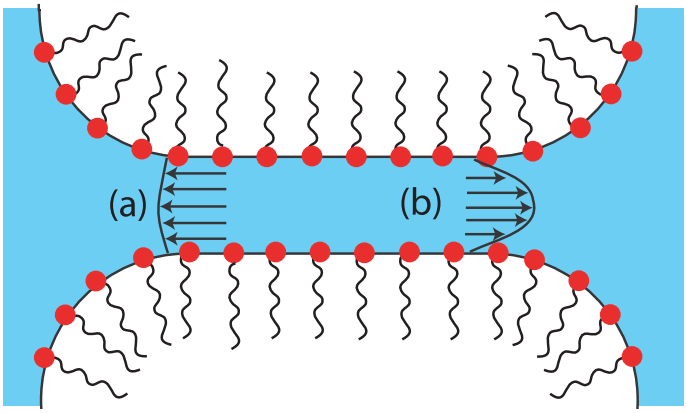

FIGURE 1.3: (a) Plug flow of liquid in thin film due to mobile surfactants: the flow slips with respect to the foam films. (b) Poiseuille flow of liquid in thin film due to immobile surfactants: the liquid experiences a no-slip boundary condition at the foam films and energy is dissipated in the shear flow near the interface.

stabilised by mobile surfactants, an uniform surface tension can easily be restored by diffusion of bulk surfactant molecules to the interface and diffusion on the surface of adsorbed molecules. There is little dissipation at the interfaces and the liquid exhibits plug flow. Immobile surfactants have a far lower diffusivity and resist flow, so the liquid flow velocity decreases steeply close to the interface, resulting in high dissipation and a Poiseuille flow profile. Foams stabilised by immobile surfactants hence drain much slower than foams stabilised by mobile surfactants. At the end of the 90's, a controversy between foam researchers at Harvard [4] and Trinity College [5] in Dublin over the drainage velocity in foams was resolved only when they realised that the different experimental results might well be due to the different dishwashing liquids used. Indeed, it turned out that the American brand Dawn has a lower surface viscosity, which is a quantity that phenomenologically describes the influence of a high Gibb's elasticity in the film, than its European counterpart Fairy (known as Dreft in the Netherlands).

Coarsening. The diffusion of water soluble gasses through the thin soap films separating bubbles leads to coarsening. This is because the capillary pressure inside the smaller bubbles in a foam is higher than in the larger

bubbles (see section 1.2.2), so that gas will mainly diffuse from the smaller to the larger bubbles. As a result, the larger bubbles will grow while the smaller bubbles shrink. A common choice of gas to slow down the coarsening process is C_2F_6, which is almost insoluble in water. A much more soluble but frequently used gas is N_2, which still performs better than air and CO_2 which easily diffuse through the foam films. Note that diffusion by soluble gases can be halted by the addition of only trace amounts of insoluble gases: the soluble gasses easily diffuse from the smaller to the larger bubbles, but since the insoluble gasses remain where they are, the concentration of insoluble gas in the smaller bubbles increases, which quickly leads to a balancing diffusion from the larger to the smaller bubbles to restore the equilibrium in gas concentration between the bubbles. This is the same mechanism that drives osmosis in cells.

Coalescence. Bubbles end their existence by rupture or coalescence with a neighbour. If the films become thin due to drainage, thermal fluctuations will eventually lead to fluctuations in the film thickness that cannot be restored anymore and will lead to rupture of the films. A way to promote rupture is by adding anti-foaming agents to the foam. These consist of oil droplets or solid particles that attach to the thin films and then due to their wetting properties, lead to a retraction of the foam film and hence to rupture. Trying to do the laundry with dishwashing soap will, due to the absence of anti-foaming agents, result in large amounts of foam in and around your washing machine. However, this could be avoided simply by adding some cooking oil.

1.2 Mesoscopics: Shape, Forces and Pressures

In the following section, we will consider the various pressures and forces that are exerted on single bubbles and foam films. We will begin by stating the rules describing a static foam configuration. Then we discuss how bubbles are deformed by compression of other bubbles or by drainage of liquid from the foam, and we discuss the forces that a bubble experiences when it is moving with respect to another bubble or a solid wall. We finally discuss the flotation forces that bubbles experience when floating at an interface, and that hence only apply to two-dimensional foams.

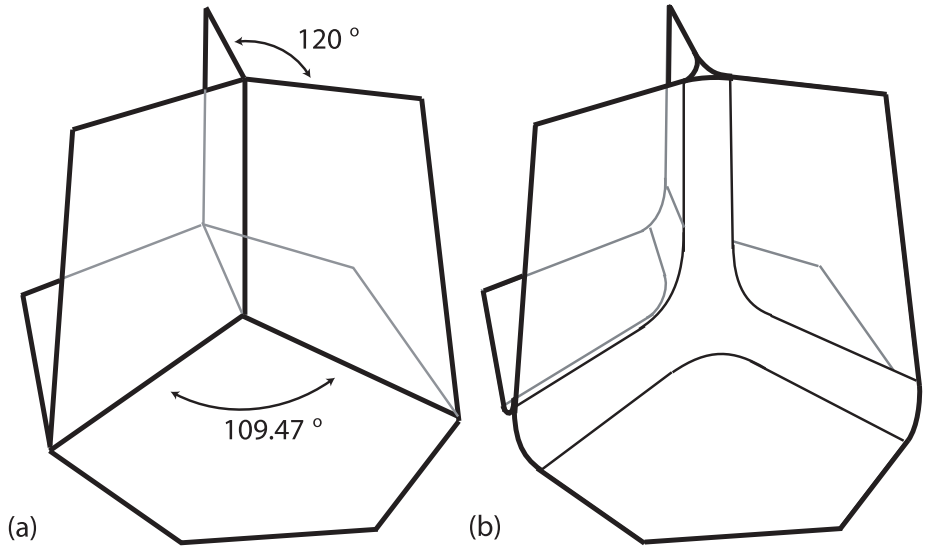

FIGURE 1.4: (a) The first and second rule of Plateau illustrated with a dry foam. Any three soap films meet at 120° angles, while three of such vertices meet in a fourfold node at an angle of 120°. (b) The same view, but for a wetter foam: the Plateau borders are decorated with circular segments .

First we need to introduce the bubble volume fraction ϕ defined as:

$$\phi_l = \frac{V_g}{V_l + V_g}, \tag{1.4}$$

with V_l and V_g are the volumes of liquid and gas respectively. In foam research people often use the liquid fraction $\phi_l = 1 - \phi$ to characterize their foam. Note that we will use the volume fraction ϕ throughout this work, to facilitate the connection with simulation results and granular experiments. A *wet* foam contains a high volume fraction of liquid and the bubbles are only weakly deformed. A typical volume fraction for a commercial three-dimensional foam such as Gilette shaving foam is $\phi = 0.80$. At $\phi = 0.64$ the foam loses its rigidity (unjams) [6, 7] and for yet lower ϕ one speaks of *bubbly liquids*. A *dry* foam consists essentially of a network of thin films and typically $\phi \approx 0.99$.

For three-dimensional foams, this liquid fraction is a well defined quantity. However, both experimentalists and theorists often retreat to two

dimensions [8–12] to study foams. The question is whether a two-dimensional liquid fraction can be defined as well. In numerical studies of two-dimensional foams, where the bubbles are represented by discs, this is no problem. Experimentally, however, this geometry is only achievable with Langmuir foams, which are monolayers of molecules that float at the surface of a liquid and aggregate into two dimensional discs. Due to the simplicity of production and imaging, physicists often prefer to work with monolayers of foam bubbles instead. However, these bubbles extend in three dimensions and since they are more or less spherical, a two-dimensional liquid fraction would strongly depend on the height at which one decides to make a slice through the bubble layer.

In this thesis we describe work performed with two-dimensional foams. We will describe the characterisation of ϕ in quasi two-dimensional foams in much more detail in chapter 4, and we will also show that in order to convincingly explain our findings we have to take into account the physics at the (three dimensional) bubble scale.

1.2.1 Plateau rules

We consider a three dimensional dry foam to establish the geometric rules at equilibrium, see Fig. 1.4(a) which where first described by Joseph Plateau. The first rule states that exactly three soap films always meet at so-called Plateau borders at angles of 120°. The second rule states that four of these Plateau borders meet at nodes under angles of 109.47°. These rules are a direct consequence of the fact that the surface tension of all films should balance at equilibrium. If we consider a two dimensional foam, i.e., a collection of lines that are pulled by surface tension, only Plateau's first rule applies. For slightly wetter foams, Plateau's rules still hold exactly, but the vertices are "decorated" with curved segments that are dictated by the Laplace pressure across the film. For still wetter foams the decorations of the vertices start to overlap and Plateau's rules no longer apply: for example, fourfold vertices become stable [1].

1.2.2 Capillary and Disjoining pressure

The shape of a liquid-gas interface is governed by the Laplace equation, which relates the pressure drop across the interface — which is called the Laplace or capillary pressure — to the surface tension σ and the principal

radii of curvature R_1 and R_2 of the interface:

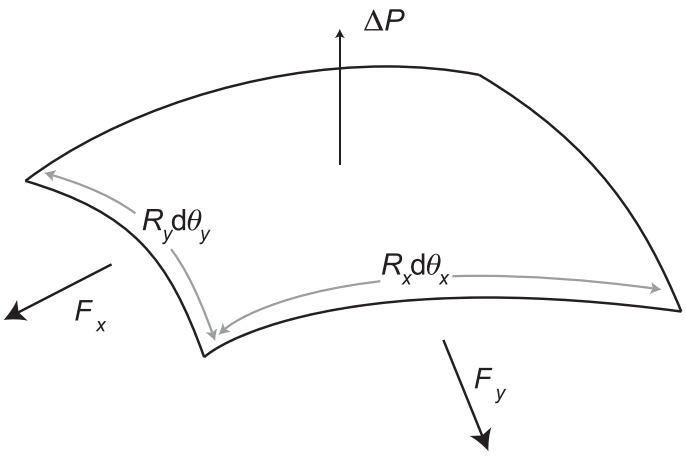

FIGURE 1.5: Illustration of surface element under a pressure gradient. If the surface curves the perpendicular component of the force due to surface tension cancels the pressure gradient.

$$P_c = P_{gas} - P_{liq} = \sigma(\frac{1}{R_1} + \frac{1}{R_2}). \tag{1.5}$$

This equation can be understood by considering an infinitesimally small surface on which surface tension acts and along which a pressure gradient ΔP exerts a force, see Fig. 1.5. The resulting force $\Delta P R_x d\theta_x R_y d\theta_y$ can only be balanced by a surface tension if the surface is curved. In that case the out of plane component of the force due to surface tension balances the pressure gradient.The restoring forces due to the surface tension pulling in the x and y directions are given by:

$$F_x \cdot \sigma \sin d\theta_x = R_y d\theta_y \cdot \sigma \sin d\theta_x \approx R_y d\theta_y \cdot \sigma d\theta_x, \tag{1.6}$$

$$F_y \cdot \sigma \sin d\theta_y = R_x d\theta_x \cdot \sigma \sin d\theta_y \approx R_x d\theta_x \cdot \sigma d\theta_y \ . \tag{1.7}$$

Balancing the force due to the pressure gradient with the restoring force due to surface tension yields:

$$\Delta P = \frac{F_x + F_y}{R_x d\theta_x R_y d\theta_y}, \tag{1.8}$$

and since $R_x = R_1$ and $R_y = R_2$ we arrive at Eq. (1.5). For a spherical bubble $R_1 = R_2$ and the capillary pressure reduces to:

$$P_c = \frac{2\sigma}{R}. \tag{1.9}$$

The consequence of Eq. (1.9) is that the gas pressure inside bubbles is inversely proportional to their size, which leads to diffusion from the smaller to the larger bubbles. This is the mechanism behind coarsening. An elegant and rigorous derivation of Eq. (1.5) is given in chapter 2 of [3]. A few additional remarks about the radii of curvature are made in Appendix 1.A.

One other pressure plays an important role at gas-liquid interfaces, and to introduce it let us consider a bubble that is pressed against a solid wall by some external force(See Fig. 1.6(a)). A flattened film results, of which we will determine the size as a function of force in Section 2.2.1, and for small deformations the pressure inside the bubble is still determined by the undeformed radius of the bubble:

$$P_{gas} = P_{liq} + P_c = P_{liq} + \frac{2\sigma}{R}. \tag{1.10}$$

At the flattened film the radius of curvature R is infinite and hence the capillary pressure is zero. There Eq. (1.10) cannot hold and a new force comes into play once the distance between the bubble and the wall becomes sufficiently small. At the film this **disjoining pressure** Π, which is a function of the film thickness h, balances the pressure difference across the surface:

$$P_{gas} = P_{liq} + \frac{2\sigma}{\infty} + \Pi(h). \tag{1.11}$$

The disjoining pressure results from the attractive and repulsive forces in the thin film, of which the electrostatic and steric repulsion have already been mentioned. An overview of surface forces that can contribute to the disjoining pressure is given in [13]. For aqueous films the disjoining pressure is often a superposition of electrostatic repulsion and a van der Waals attraction. A typical shape of the $\Pi(h)$ dependence in this case is shown in Fig. 1.6(b). For very short distances a short range Born repulsion is added.

From Eq. (1.11) it is clear that at equilibrium $P_c = \Pi(h)$ so the equilibrium film thicknesses are given by the roots of this equation. As shown in Fig. 1.6(b), there are three equilibrium film thicknesses. At point 1, the

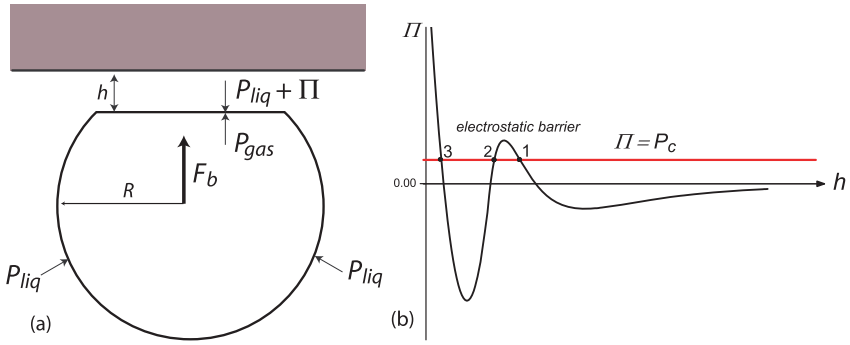

FIGURE 1.6: (a) Pressure balance for deformed bubble, pushed against a solid boundary by buoyancy. At the flattened facet the radius of curvature is ∞ and P_c needs to be balanced by a disjoining pressure Pi. (b) Disjoining pressure isotherm. The horizontal line corresponds to equilibrium film thicknesses. Point 1 and 2 represent *common* and *Newton black film* thicknesses.

film is called *common black film* and there it is stabilised by double layer repulsion. A common black film is defined as being at least thinner than 1/4 of the wavelength of visible light but thicker than 7 nm. Point 2 is an unstable equilibrium and is never observed in experiment and Point 3 corresponds to the *Newton black film*, which is stabilised by the short range Born repulsion. Newton black films are thinner than 7 nm.

1.2.3 Bubble deformation

Bubble deformation by compression

If a bubble is pressed against another bubble or a solid or liquid interface, at equilibrium (or quasi-equilibrium) the driving force is balanced by the disjoining pressure in the resulting thin film [14]:

$$\pi r_c^2 \Pi = F, \tag{1.12}$$

where πr_c^2 is the area of the flat film. Note that at quasi-equilibrium, for a thinning film, this disjoining pressure can also contain a viscous pressure contribution. The liquid and gas pressures cancel when integrated over the bubble surface and do not result in forces. In principle a transversal tension, which is due to the surface tension imbalance at r_c (where

the bubble surface curvature suddenly changes) should be included in Eq. (1.12). However, this tension is generally considered to be negligibly small [3, 14].

In Fig. 1.6(a) the bubble is driven upwards by buoyancy and the force balance reads:

$$\pi r_c^2 \Pi = F = \frac{4}{3}\pi R_0^3 \Delta\rho g, \tag{1.13}$$

with R_0 the bubble radius, $\Delta\rho$ the density difference between gas and liquid phase and g the gravitational acceleration.

We will now derive an expression for the force on the bubble in terms of measurable quantities such as the bubbles radius R_0, the surface tension σ and the radius of the deformed facet r_c. From Eq. (1.11) we know that for small r_c, such that the gas pressure remains constant, the disjoining pressure Π is balanced by the capillary pressure P_c. We can thus rewrite Eq. (1.12):

$$F = \pi r_c^2 P_c = \pi r_c^2 \frac{2\sigma}{R_0}. \tag{1.14}$$

In an experimental situation [15, 16] the interparticle force F_{ij}, which is the sum of the forces F_i on particle i and F_j on particle j, can hence be deduced from the size of the flattened film separating the two bubbles pressing against each other by the above reasoning (See Fig. 1.7):

$$F_{ij} = F_i + F_j = \pi r_c^2 \Pi = \pi r_c^2 [(P_c)_i + (P_c)_j] = \pi r_c^2 2\sigma \frac{R_i + R_j}{R_i R_j}. \tag{1.15}$$

The compressive force can be related not only to the area of the deformed facet, but also to the deformation itself, through a force law. To extract this force law for the bubbles, we can consider the deformation $\delta\xi$ [17], where $\xi = (R_0 - Z)/R_0$ is a dimensionless measure of compression (See Fig. 1.8). For small deformations, to linear order in $\delta\xi$:

$$r_c^2 \approx 2R_0^2 \delta\xi. \tag{1.16}$$

We can now insert this in Eq. (1.14) and obtain

$$F \approx 4\pi\sigma R_0 \delta\xi. \tag{1.17}$$

To good approximation, the interaction between bubbles can thus be taken as a repulsive harmonic potential. If a bubble is compressed by many neighbouring bubbles and the deformed surface area becomes large, this approximation breaks down and the interbubble interaction becomes stiffer than harmonic [17].

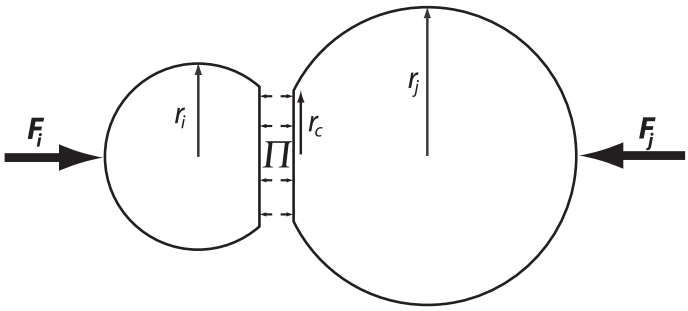

FIGURE 1.7: Illustration of the relation between force on bubbles and deformed facet: the exterted forces F_i, F_j are balanced by the disjoining pressure Π, which can be expressed in terms of the Laplace pressure P_c.

Bubble compressed by buoyancy

If a bubble is trapped under a solid boundary and pushed upwards, and hence deformed by gravity, we can extract r_c by combining Eqs. (1.13) and (1.14), provided that the bubble radius is smaller than the capillary length $\kappa^{-1} = \sqrt{\frac{\sigma}{\rho g}}$. In this case we find:

$$r_c = \sqrt{\frac{2}{3}} \frac{R_0^2}{\sqrt{\frac{\sigma}{\rho g}}} = \sqrt{\frac{2}{3}} \frac{R_0^2}{\kappa^{-1}}. \tag{1.18}$$

However, when the bubble radius is larger than κ^{-1} the bubbles adopt a "pancake" shape with the length of the short axis given by $2\kappa^{-1}$. In that case the contact radius can be found by considering that the bubble volume is conserved after deformation: $\frac{4}{3}\pi R_0^3 = 2\pi r_c^2 \kappa^{-1}$. Hence:

$$r_c = \sqrt{\frac{2}{3}} \frac{R_0^{3/2}}{\kappa^{-1/2}}. \tag{1.19}$$

These scalings were measured to hold approximately in [18] but here we will show they are exact and excellently match experimental data. We measured the contact radius as a function of R_0, by blowing N bubbles of a certain radius R_0. Since the bubbles are not spherical as they float at an interface, we determine this radius by measuring the amount of space they occupy in an upright tube of 1x1x20 cm, see Fig. 1.9(b). We then tilt

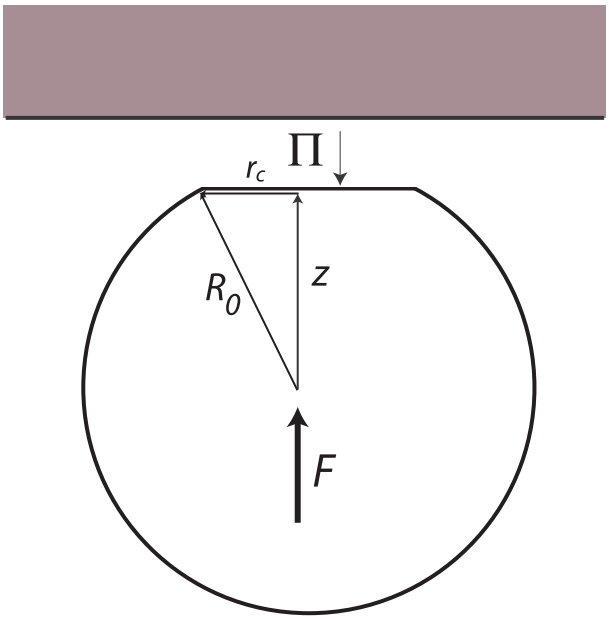

FIGURE 1.8: Pressure balance for deformed bubble: the dimensionless overlap $\xi \equiv (R_0 - z)/R_0$ can be expressed in terms of r_c.

the tube by 90 degrees and measure r_c by looking at the reflection of a light source by the flattened facet. We used Dawn as surfactant, for which we measured $\sigma = 28 \pm 1$ mN.m^{-1}. The results are plotted in Fig. 1.9(a): the theoretical expression fits excellently to the data for $\kappa^{-1} = 1.62 \pm 0.02$ mm, which is within error bars to the result $\kappa^{-1} = 1.64 \pm 0.06$ mm obtained from measuring σ.

Finally we remark that if the density difference between the bubble phase and the liquid phase is small (as can be the case for emulsions), bubbles remain essentially undeformed. This can easily be seen from Eq. (1.18): r_c scales quadratically with bubble radius.

Bubble deformation by drainage

Liquid mainly drains from the foam via the Plateau borders. As a consequence, due to the decreasing liquid fraction, the foam bubbles deform and the Plateau border radius of curvature decreases, see Fig. 1.10, re-

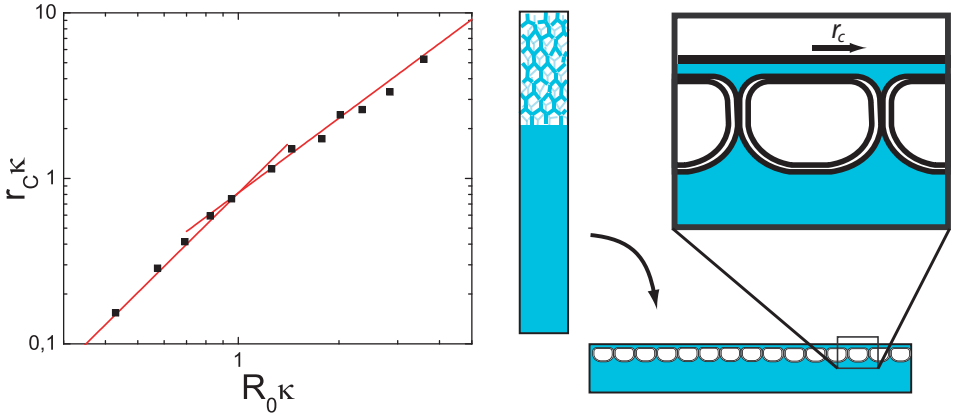

FIGURE 1.9: (a) Measured dependence of the radius of the flattened contact normalised by the capillary length versus the undeformed bubble radius normalised by the capillary length. Solid lines are the theoretical results from Eqs. (1.18) and (1.19) for $\kappa = 1.62$ mm.

sulting in an increase in the capillary pressure. To good approximation, the gas pressure inside the bubbles remains constant and hence the liquid pressure in the Plateau border must decrease to satisfy the Laplace equation. The resulting pressure gradient between the foam films and the Plateau border causes liquid to be sucked from the thin films separating the bubbles, where the liquid pressure is higher, to the Plateau border where the pressure is lower, which leads to thinning.

1.2.4 Viscous drag forces

Bubbles that move with respect to other bubbles or a wall experience viscous drag forces due to the resistance to flow of liquid in the thin films separating the bubble from a neighbour or a wall. This resistance to flow is linked to the concepts of surface elasticity or viscosity we have introduced before. The interaction between a moving bubble and a wall has been extensively studied, both theoretically [19–21] and experimentally [18, 20–22]. The frictional force F_{bw} turns out to scale as:

$$F_{bw} \propto (Ca)^n, \tag{1.20}$$

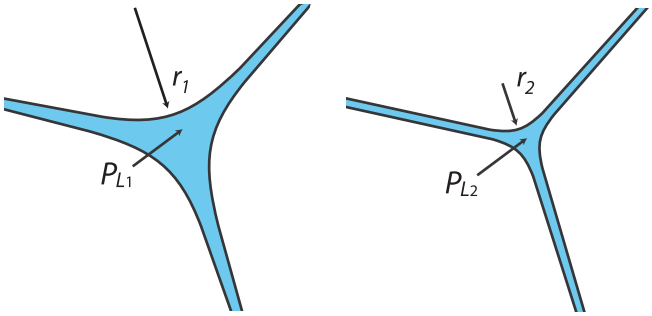

FIGURE 1.10: Due to drainage of the fluid the Plateau border radius of curvature decreases. This leads to a decrease in the liquid pressure and as a result, liquid is sucked from the films, leading to thinning.

with Ca the capillary number, describing the ratio of viscous and surface tension contributions to the force, given by $(Ca) = \eta v/\sigma$, with, η the viscosity, v the relative bubble speed and σ the surface tension. The power law index n depends on the mobility of the surfactants that stabilize the foam films: for mobile bubble surfaces, i.e for bubble surfaces that have very low E_G, $n = \frac{2}{3}$, whereas for immobile surfaces (where E_G is high) $n = \frac{1}{2}$ [20]. The model can be refined further by including the liquid fraction of the foam in terms of the relative size of the deformed film separating the bubble and the wall: r_c/r_{PB}, where PB denotes Plateau border. For all practical purposes though, the viscous drag can be assumed to scale as in Eq. (1.20) with n somewhere between $\frac{1}{2}$ and $\frac{2}{3}$.

The viscous friction between bubbles sliding past each other is much less studied, and is often taken to scale linearly with the velocity difference between bubbles [10, 23]. A theoretical study of the viscous drag in dry monodisperse foams under shear yields a viscous drag force that scales with $Ca^{2/3}$ [24], hinting that the mechanism of viscous dissipation between bubbles that slide past one other is the same as for a bubble slipping past a wall. A very recent theoretical analysis of layers of bubbles in an ordered bcc structure [25], reveals that for immobile foams the viscous

drag force between bubbles scales as:

$$F_{bb} \propto (Ca)^{0.5}. \tag{1.21}$$

We will come back to the scaling of the viscous dissipation in much greater detail in Chapter 2.

1.2.5 Capillary forces on floating bubbles

Bubbles floating at an air/water interface will in general experience lateral forces due to the fact that neighbouring bubbles deform the water surface. The origin and functional form of these forces will be discussed in the next section. The derivation is most easily carried out for solid particles, but is equally valid for foam bubbles and emulsion droplets. The deformation of an interface $\zeta(x, y)$ in the vicinity of a floating particle is due to the requirement that the surface tension balances with gravity while simultaneously the interfacial tensions balance at the three-phase contact line. This requires the liquid phase to meet the particle under a certain angle, which results in a deformation of the surface.

Flotation forces

Two types of lateral capillary forces exist, of which we present an overview in Fig. 1.11: a capillary flotation force, which is caused by the deformation of the liquid interface due to the weight (or buoyancy) of a floating body and a capillary immersion force, which occurs if particles are partially immersed in a liquid layer and which is due to wetting of the particle. Both forces are attractive if the contact angles at the particles are of the same sign, and repulsive if they are of different sign.

Since our particles float at the surface of a deep basin of soapy solution, for our system the only relevant capillary force is the flotation force. To calculate this force we follow [3]. In this book the authors provide an excellent summary of work performed by Kralchevsky and co-workers that expands and refines the approach first taken by Nicholson [26], which is called the *linear superposition approximation (LSA)*.

Consider a particle floating at the interface between two immiscible fluids. The origin is fixed at the particle position. The force due to gravity (which consists of the particle weight as well as buoyant forces) is balanced by the vertical component of the surface tension integrated over the

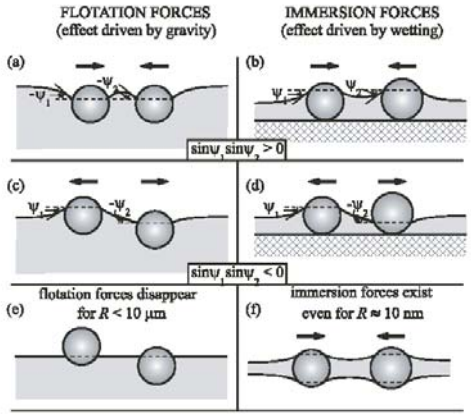

FIGURE 1.11: Flotation and immersion forces compared. Depending on the contact angle, the forces can either be attractive or repulsive. Foam bubbles will always attract, as in (a). *Figure taken from [3].*

three-phase contact (tpc) line, as is shown in Fig. 1.12:

$$F_{g(1)} = 2\pi\sigma r_1 \sin\psi_1, \tag{1.22}$$

where r_1 i the radius of the tpc line. Now we bring in particle 2 from infinity ($\zeta = 0$) to a distance L, where it is located at $\zeta(L)$ below the horizontal plane due to the meniscus created by particle 1. The work carried out by the gravitational force to bring particle 2 from $z = 0$ down to $z = -\zeta(L)$ is:

$$\Delta W_g = -F_{g(2)}\zeta(L) = -2\pi\sigma r_2 \sin\psi_2 \zeta(L). \tag{1.23}$$

Introducing the capillary charge $Q \equiv r\sin\psi$ this can also be written as:

$$\Delta W_g = -2\pi\sigma Q_2 \zeta(L). \tag{1.24}$$

Thus, before we can obtain the force on the particle from W we first have to find an expression for the meniscus deformation around particle 1. This deformation is given by Eq. (1.51) in appendix 1.A:

$$\nabla_{II} \cdot \left(\frac{\nabla_{II}\zeta}{\sqrt{1 + |\nabla_{II}\zeta|^2}} \right) = [P_2(\zeta) - P_1(\zeta)]/\sigma, \tag{1.25}$$

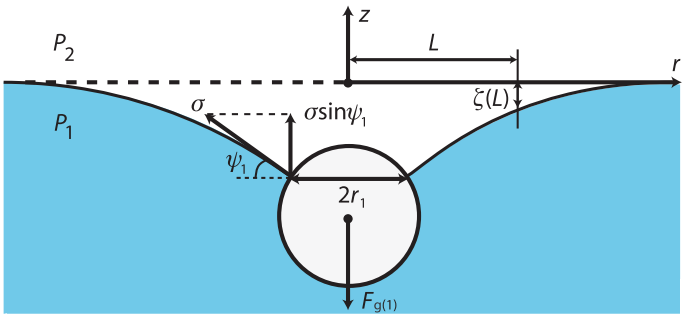

FIGURE 1.12: The force balance for a heavy spherical particle: the force due to gravity acting on the particle is balanced by the vertical component of the surface tension integrated over the three-phase contact line.

with

$$\nabla_{II} \equiv \mathbf{e}_x \frac{\partial}{\partial x} + \mathbf{e}_y \frac{\partial}{\partial y}. \tag{1.26}$$

If the buoyant and gravity forces are considerably smaller than the interfacial tension force, that is, if the Bond number $\rho g R^2/\sigma < 1$, the surface deformations around the particle are small [27]. In this case $\mid \nabla_{II}\zeta \mid^2$ becomes negligible and equation 1.51 reduces to:

$$\nabla^2_{II}\zeta = [P_2(\zeta) - P_1(\zeta)]/\sigma. \tag{1.27}$$

Now the pressures at both sides of the interface ζ can be expressed in the following form [27]:

$$P_1(\zeta) = P_1^{(0)} - \rho_1 g\zeta, \qquad P_2(\zeta) = P_2^{(0)} - \rho_2 g\zeta. \tag{1.28}$$

Here ρ_1 and ρ_2 are the densities of the respective fluid phases, and $P_{1,2}^{(0)}$ are the pressures of the respective fluid phases at $\zeta_\infty = 0$. Inserting 1.28 in 1.27 we end up with:

$$\nabla^2_{II}\zeta = \kappa^2\zeta, \qquad \kappa^2 = \frac{\Delta\rho g}{\sigma}, \qquad \Delta\rho = \rho_1 - \rho_2, \tag{1.29}$$

where $q\kappa$ is the inverse capillary length encountered before, $\kappa = \sqrt{\frac{\Delta\rho g}{\sigma}}$.

If this equation is written in cylindrical coordinates it reduces to the modified Bessel equation, whose solution is for small meniscus slope [28]:

$$\zeta(r) = AK_0(\kappa r) \tag{1.30}$$

with K_0 a modified Bessel function of zeroth order. The constant A can be determined [29]: $A = r_1 sin\psi_1 = Q_1$ with ψ the three phase contact angle.

Inserting Eq. (1.30) in Eq. (1.24) we end up with

$$\Delta W_g = -2\pi\sigma Q_1 Q_2 K_0(\kappa L). \tag{1.31}$$

Now, we know that

$$F = -\frac{d\Delta W_g}{dL}; \qquad \frac{dK_0}{dx} = -K_1(x), \tag{1.32}$$

so the capillary flotation force obeys:

$$F = -2\pi\sigma Q_1 Q_2 \kappa K_1(\kappa L). \tag{1.33}$$

It is intrinsic to the approximation that the LSA loses its validity for small inter-particle distances. It has been claimed in [30] that the LSA considerably underestimates the capillary attraction. However, recent numerical calculations [28] have shown that for small slope angles, the linear superposition approximation remains valid within 2 % up to particle contact. The authors furthermore show that for many particle systems, the forces are pair-additive.

Dependence of flotation force on particle size

The linearisation of Eq. (1.51) is only allowed if $R_0^2\kappa^2 \ll 1$. This condition is found by equating F_g with the surface tension force, as described above. For an air/water interface $\kappa^{-1} = 2.7$ mm. Furthermore it is shown in section 8.1.2 of [3] that: $Q \propto R_0^3$, with R_0 the droplet radius. Therefore the R_0 dependence for the flotation force is:

$$F \propto (R_0^6/\sigma)K_1(\kappa L) \tag{1.34}$$

This means that for bubbles close to each other a decrease of the surface tension, for instance by adding surfactant, increases the force. On the other hand the long range force, which is hidden in the Bessel function, then decreases. It also implies the flotation force becomes smaller than kT and thus smaller than the Brownian force for $R_0 <$ 5-10 μm.

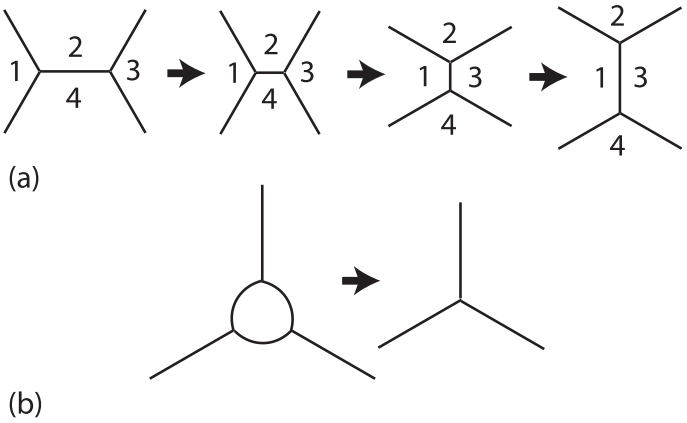

FIGURE 1.13: ((a) T1 process in a 2D foam: the film between bubbles 2 and 4 shrinks to 0, after which the unstable fourfold vertex is resolved by creating a new film between bubble 1 and 3. (b) T2 process in a 2D foam: a small bubble located at the vertex of three larger films disappears due to coarsening.

1.3 Macroscopics: structure, rearrangements and rheology

This section deals with the macroscopic behaviour of a foam under externally imposed stresses or strains. We will explore connections between the micro- and mesoscopic concepts introduced before and the macroscopic behaviour.

1.3.1 Foam structure

If one blows bubbles of one size on the surface of a soapy solution, the bubbles will, due to the flotation forces discussed above, attract and order in a hexagonal packing [31]. A foam consisting of same-sized bubbles is called a monodisperse foam and will order for bubble size variation (polydispersity) up to 10%. For larger polydispersity, a disordered foam results.

In the beginning of Section 1.2 we briefly discussed the volume fraction ϕ. For a two-dimensional hexagonal packing of discs, the jamming or rigidity loss point is at $\phi = 0.909$ [32]. A disordered disc packing, however,

jams at $\phi = 0.842$ [33]. Although in real foams bubbles mutually attract and are three-dimensional objects, we include these numbers here to highlight the structural differences between ordered and disordered foams.

A three-dimensional disordered foam unjams at $\phi = 0.64$, but a three-dimensional monodisperse foam will again form crystalline lattices at much higher volume fractions, depending on the lattice structure, which can be either FCC or BCC [34].

1.3.2 Structural rearrangements and visco-elastic behaviour

The response of a bubble to deformations and the viscous dissipation between two bubbles during flow was discussed in section 1.2. How these forces at the bubble scale translate to the bulk scale is largely unknown and constitute the focus of this thesis, but as a result of the interplay of these nonlinear interactions and the disordered flow of the foam, the bulk response of a foam is highly nontrivial. For small applied strains, bubbles want to restore their equilibrium surface area, and foams respond elastically, i.e.like a solid [1]. If the strain is increased the foam deforms plastically: it relaxes the stresses through bubble rearrangements [1, 32]. For large and continuously applied strains, the foam flows irreversibly with bubbles rearranging continuously [35, 36]. The flow of foams is often measured in oscillatory rheological measurements [7, 37, 38] and fit to certain flow models, which we will describe in the following section.

For a dry foam the bubble rearrangements through which a foam flows are well defined, and two elementary topological processes have been identified that drive the structural evolution of the foam: the T1 and T2 processes, see Figs. 1.13(a)+(b). A T1 process denotes the neighbour swapping of bubbles and is most easily explained for a two dimensional foam, see Fig. 1.13(a): the facet between bubbles 2 and 4 shrinks to zero, resulting in a fourfold vertex. In such a vertex the surface tensions cannot be stably oriented; this instability is resolved with the creation of a new facet between bubble 1 and 3. The T2 process corresponds to the disappearance of a small bubble located at a vertex due to coarsening, see Fig. 1.13(b), and is hence not connected to stress induced evolution of the foam. For wet foams, topological rearrangements seem less well defined, although attempts have been made to treat wet foams within this picture of topological rearrangements by simply considering a wet foam as a dry foam, the vertices of which are decorated with circular arcs [32, 39]. It remains

an open question whether considering the flow of foams entirely through T1 processes is a valid tool for realistic, experimental foams.

Elastic, viscous and visco-elastic response

For an elastic medium, the shear stress τ and the shear strain γ are related through:

$$\tau = G\gamma, \tag{1.35}$$

with G the shear modulus. For a fluid that is sheared between two plates with a strain rate $\dot{\gamma}$ the relation between stress and strain reads:

$$\tau = \eta\dot{\gamma}, \tag{1.36}$$

with η the viscosity.

As was discussed before, foams exhibit both solid and liquid properties and are hence said to be visco-elastic materials. The simplest way to describe this visco-elastic behaviour in terms of a relation between the strains and the stresses is by simply combining both expressions for the stresses. The two simplest procedures to do so are due to Kelvin and Maxwell and are obtained by modeling the elastic response by a spring with stiffness G and the viscous response by a dashpot, characterized by η. In the Maxwell model the spring and the dashpot are placed in series and since the total strain is the sum of the strains on the dashpot and spring, we can write:

$$\gamma = \gamma_1 + \gamma_2 = \frac{\tau}{G} + \frac{\tau}{\eta} \cdot t. \tag{1.37}$$

The Maxwell model captures the behaviour of a fluid under a step stress, with an instaneous elastic response plus a permanent creep flow.

The Kelvin model models a different kind of response and can thus be applied to different systems. In this model, the spring and the dashpot are placed in parallel and this time the stresses over each element are added up, resulting in:

$$\tau = \tau_1 + \tau_2 = G\gamma + \eta\dot{\gamma}. \tag{1.38}$$

More complex models involve many springs and dash-pots, can deal with both step stresses and step strains and are used to model more realistic systems [40–43].

Rheometry and complex shear modulus

If one is interested in the rheological response of a viscoelastic medium over a wide range of time scales, sweeping a periodically varying strain over many decades in frequency yields the desired information, as opposed to imposing a step strain or step stress as in the models discussed above. Imposing a periodically varying strain:

$$\gamma = \gamma_0 \sin \omega t \tag{1.39}$$

yields a stress:

$$\tau = \tau_0 \sin(\omega t + \delta). \tag{1.40}$$

The phase shift δ can be understood by considering the response of purely elastic material, for which $\delta = 0$, and that of a viscous fluid for which:

$$\tau = \eta\dot{\gamma} = \eta\gamma_0\omega \cos \omega t = \tau_0 \sin(\omega t + \frac{\pi}{2}), \tag{1.41}$$

hence $\delta = \frac{\pi}{2}$. For a visco-elastic material, the phase-shift will be somewhere between 0 and $\frac{\pi}{2}$ and the stress can be written as:

$$\tau = \tau_0 \sin(\omega t + \delta) = (\tau_0 \cos \delta) \sin \omega t + (\tau_0 \sin \delta) \cos \omega t. \tag{1.42}$$

This shows that there are two components to the stress, one in phase with the deformation and one with a phase difference of 90°. One then defines the *storage* and the *loss* modulus G' and G'' as:

$$G' = \frac{\tau_0}{\gamma_0} \cos \delta \equiv G_0 \cos \delta, \tag{1.43}$$

$$G'' = G_0 \sin \delta \tag{1.44}$$

and write the stress as:

$$\tau = \gamma_0(G' \sin \omega t + G'' \cos \omega t). \tag{1.45}$$

The storage modulus G' is the amplitude of the in-phase component of the response and is a measure of the energy that is reversibly stored in the material, hence the elastic energy, while the loss modulus G" is the out-of-phase component and denotes the viscous dissipation per oscillation. Writing the strain as $\gamma = \gamma_0 \exp(i\omega t)$, the complex shear modulus becomes:

$$G^* = G' + iG''. \tag{1.46}$$

Constitutive equations

Rheometrical data are often fit to constitutive equations. For Newtonian fluids, the constitutive equation is simply Eq. (1.36). However, to account for the solid-like behaviour, foam rheology is often fit to the Bingham model [44], which accounts for the experimentally observed fact that below a certain stress, called the yield stress, the foam does not flow but responds elastically. The Bingham model reads:

$$\tau = \tau_Y + \mu\dot{\gamma}, \tag{1.47}$$

with τ_Y the yield stress and μ the consistency. The model has a linear dependence of the stress with the strain rate, like a Newtonian fluid.

The Herschel-Bulkley model [45]is similar to the Bingham model, but allows for a non-linear scaling of the viscosity:

$$\tau = \tau_Y + \mu\dot{\gamma}^n. \tag{1.48}$$

If $n > 1$ the material exhibits *shear-thickening* behaviour, that is, it becomes more viscous the faster its driven. On the other hand, if $n < 1$, as is the case for foams [20, 46, 47], the material is *shear-thinning*: it flows more easily for higher driving rates. While the inclusion of a yield stress term in a constitutive equation describing foam rheology appears to be a natural way to describe the elastic response of the system, a microscopic justification for linear or non-linear scaling of the foam viscosity is at present lacking.

1.4 Experiments and numerics on foams and emulsions

1.4.1 Experiments

The first experiments on foam and emulsion rheology stem from the eighties, and since then physicists have mainly studied the rheology of three-dimensional foams and emulsions in Taylor-Couette geometries [32, 35, 38, 46, 48–51]. While these measurements have shed light on the highly non-trivial bulk properties of foams and emulsions, relationships between bulk rheology and behaviour at the bubble scale remained elusive. Recent results, obtained using novel imaging techniques such as DWS [52]

x-ray tomography [53] and confocal microscopy [15, 16] start to elucidate this highly non-trivial connection between local and bulk scale. However, many questions remain unanswered, and we hope these can be addressed by performing experiments on two-dimensional foams. An overview of two-dimensional foam flow experiments is given in chapter 2.

1.4.2 Numerics

The numerical modeling of foam statics and rheology is carried out using a wide variety of techniques, all of which capture part of the rheological behaviour. One of the first simulations was carried out with the PLAT code [33], in which a foam is constructed by creating a Voronoi tessellation and relaxing it to equilibrium, all the while satisfying the Laplace pressure equation for each bubble. The wetness is varied by repeating this procedure while replacing the vertices by circular arcs, and finally this foam of variable wetness is sheared. The strain is increased in small increments and the foam is allowed to relax to static equilibrium between each increment. Such a foam is said to be in the *quasistatic limit*.

The structure of a dry foam can be generated by the surface minimisation routine Surface Evolver, developed by Ken Brakke [54], which is intrinsically quasistatic and which can be adapted to simulate shear flow of dry foams. The vertex model [55] is also limited to dry foams, since it models the Plateau-borders as straight lines, but it includes a linear viscous dissipation in the foam films. The viscous froth model [56], developed recently, can be implemented either in the Surface Evolver framework or in the PLAT code to explicitly describe the presence of confining glass plates through a viscous drag force acting on the entire Plateau border.

The soft disc or bubble model [23, 57, 58] focusses on wet foam behaviour, as it models foam bubbles as spheres that repel each other harmonically and experience a viscous drag proportional to their velocity difference when sliding past each other. It predicts a Bingham behaviour for the rheology and since ϕ can be varied, it uncovers non-trivial scaling of the bulk and shear moduli B and G with ϕ.

Finally, the cellular Potts model [59], in which bubbles are represented by patches of numbers that obey certain rules involving the numerical values of neighbouring patches, is well suited to simulate coarsening in dry foams [60] and has in a few instances been modified to accomodate

the simulation of shear flow [61].

These simulation techniques can each be used to model only parts of the foam behaviour encountered in experiment. For instance, the distribution of stress drops in bubble raft experiments has been found to be in agreement with predictions made in the bubble model [8]. Foams simulated as a collection of vertices — i.e a dry foam — in a Couette geometry display shearbanding, both in quasistatic [62] simulations and in viscous froth [11] simulations, similar to the flow behaviour observed in experimental dry foams. In the viscous froth simulation, however, the exerted rate of strain determines the location of the shearband (and hence of the T1 events): for infinitely slow shear the T1's are located at the cylinder that is not rotated whereas for higher strain rates the T1's are located close to the rotating cylinder.

1.4.3 Differences between foams and emulsions

While emulsions and foams share many properties, these systems exhibit a few differences, which we will now discuss At the smallest scale, the interfacial rheology of the adsorbed monolayers of soap molecules is different because the fluid inside emulsions droplets can flow, hence dissipating energy [3], whereas in foams the air inside bubbles does not dissipate energy.

Furthermore, experimentally three-dimensional emulsions can be made in such a way that they transmit light by index matching the bulk and the dispersed liquid [15, 16]. As a result, the three-dimensional structure can be probed directly with confocal microscopy. In addition, emulsion droplets can also be density matched with the bulk fluid to eliminate of the effects of gravity.

The main difference between emulsions and foams is due to the size of the constituent particles: as a result of the way emulsions are produced, and to meet stability requirements, emulsion droplets are often in the micrometer size range, resulting in Brownian motion. At that scale emulsion systems are most directly related to colloidal systems: for instance, they undergo a glass transition at $\phi = 0.58$ [46]

A phenomenon which occurs in emulsions is flocculation: in absence of a confining pressure, emulsion droplets still deform and form extended connected conglomerates called flocs, due to long-range attractive forces, caused by depletion attractions [63]. Whether such a depletion attraction

might exist in foams stabilised with surfactant solutions well above the CMC is an open question. Finally a few remarks about differing jargon between emulsions and foams: Coarsening is often called *Ostwald ripening* in emulsions. Drainage is referred to as *creaming*.

Appendix 1.A Laplace equation of capillarity

The shape of a liquid surface is governed by the Laplace equation of capillarity, written here in Cartesian coordinates:

$$\frac{(1+\zeta_y^2)\zeta_{xx} - 2\zeta_{xy}\zeta_x\zeta_y + (1+\zeta_x^2)\zeta_{yy}}{(1+\zeta_x^2+\zeta_y^2)^{3/2}} = [P_2(\zeta) - P_1(\zeta)]/\sigma, \tag{1.49}$$

where ζ_i denotes derivatives with respect to the i-th coordinate, P_j is the pressure of phase j and σ is the interfacial tension. A very elegant derivation of (1.49) is given in chapter 2 of [3]. Writing the left hand side of (1.49) more elegantly we arrive at:

$$2H\sigma = P_2(\zeta) - P_1(\zeta) \tag{1.50}$$

with H given by:

$$H \equiv \nabla_{II} \cdot \left(\frac{\nabla_{II}\zeta}{\sqrt{1+\mid \nabla_{II}\zeta \mid^2}} \right), \tag{1.51}$$

$$\nabla_{II} \equiv \mathbf{e}_x \frac{\partial}{\partial x} + \mathbf{e}_y \frac{\partial}{\partial y}. \tag{1.52}$$

H is a basic quantity in differential geometry called the *mean curvature*. This quantity can also be expressed through the principle radii of curvature of the surface R_1 and R_2:

$$H = -\frac{1}{2}\left(\frac{1}{R_1} + \frac{1}{R_2}\right). \tag{1.53}$$

Inserting this in (1.50) we recover the familiar form of the Laplace equation:

$$\sigma\left(\frac{1}{R_1} + \frac{1}{R_2}\right) = P_2(\zeta) - P_1(\zeta). \tag{1.54}$$